Feasibility study on the micro-forming of novel metal foil arrays based on submerged cavitating water-jet impingement

Fuzhu Li (lifuzhu01@sina.com)
Jiangsu University
Ying Yan
Kun Zhang
Yi Ren
Lihui Ren
Honglei Ma
Yun Wang
Peiyu He

Research Article

Keywords: Cavitating water-jet, Cavitation collapse, Impact, Metal foil, Micro-array forming

Posted Date: February 10th, 2022

DOI: https://doi.org/10.21203/rs.3.rs-1311564/v1

Abstract

To solve the problems of high cost and complex technology in the current plastic forming method of metal foil, a micro-forming method of submerged cavitation water-jet metal foil array with cavitation collapse shock wave loading is presented in this paper, which has advantages of high efficiency, flexibility, low cost and environmental protection. 304 stainless steel foil array micro-pore formation was taken as an example in this paper. The mixing nozzle was designed and three regions where the cavitation water-jet acts on were analysed. The influence law of target distance, impact time on the forming depth and uniformity of metal foil array was examined and the optimal position of array micro-forming in the impact zone of vacuoles collapse was revealed. Results indicate that the depth and uniformity of array micro-pores in the impact zone of cavitation collapse increases with time. However, with the increase of the target distance, it will increase first and then decrease; the depth of the array micro-pores on the radius r=13.6 mm can reach 166.4 μm, and the variance is only 5.9 μm under the condition of impact time of 5 min, target distance of 120 mm and pressure of 20 MPa; the maximum surface roughness is 1.54 μm and the thinning rate is between 2% and 10%.

1 Introduction

With the rapid development of MEMS (Micro-electro-mechanical system) technology, the light, small, thin and multifunctional micro devices have a tendency to be miniaturised and complicated. Metal foil array micro plastic forming devices are increasingly used in electronic information, aerospace, rail transit, biomedical and other fields [1, 2]. Micro plastic forming of metal foil array with the advantages of its low cost, high efficiency and good performance in the process of producing, which becomes one of the effective ways to solve the construction and manufacturing of lightweight materials and high-performance foils. It also represents the forefront of the development of modern manufacturing science [3].

The research on the micro-forming of metal foil is focused on the forming methods of micro deep drawing, micro incremental forming, micro bending, micro blanking and micro bulging. These micro plastic forming technologies integrate the advantages of traditional plastic forming. However, some problems such as the difficulties of mould manufacturing, high friction resistances, high difficulties in positioning and unclear forming mechanism caused by micro-scale effect remain, which seriously limits its industrialisation [4, 5]. In addition, the traditional micro plastic forming technology is used in the micro plastic forming of high temperature, titanium and amorphous alloys. It is difficult to achieve the high requirements of dimensional accuracy and micro-structure and properties in the form of collaborative foil micro-forming [6]. Ultrasonic, pulsed current, laser, electromagnetic and other special physical field-assisted micro-forming methods of composite foil have been developed rapidly. However, the complex manufacturing process, long cycle, large investment, environmental pollution and poor repeatability cause difficulty in adapting to batch and flexible production [7, 8]. Therefore, it is urgent to explore new plastic forming methods of metal foil that is used to solve the current problems of array micro plastic forming.

Submerged cavitating water-jet is a high-pressure water jet that has passed through the nozzle and then forms a large number of cavitating water jets under the complex conditions of confining pressure. Additionally, strong shear, GPa and 100-meter-high energy micro jet will be produced when it collapses on or near the solid surface [9]. Therefore, it is widely used in cleaning, sewage treatment, geotechnical mining and other fields [10–12]. The application of cavitating water-jet to surface modification has aroused researchers' interests in recent years. Among them, the research on cavitation water-jet peening of copper, aluminum and stainless steel by the Soyama team is the most representative as it reveals the influence of nozzle structure, injection pressure and target distance on the micro-structure of materials and achieves fully satisfactory results [9]. Tsuda et al. [13] combined with quenching treatment. Cavitation water shot peening was used to strengthen the spiral gear made of carbon steel. It formed a 100 μm deep reinforced layer and a residual compressive stress of 600 MPa. Saito spearheaded the research on sheet metal forming with cavitating water jet. Results show that high-speed plastic deformation of sheet metal occurs under the impact of cavitation collapse [14]. Tie-Niu et al. [15] proposed a new laser-induced cavitation forming process, punched out square pits with a side length of 500 μm and circular pits with a diameter of 500 μm. However, few reports exist on the application of cavitating water-jet to micro plastic forming of metal foil arrays.

This paper is based on the surface modification of cavitating water jet materials and relevant theories. Innovativeness loads the cavitation water-jet cavitation collapse micro-jet shock wave onto the metal foil surface to explore the array micro-forming method of metal foil under the impact of submerged cavitating water-jet. 304 stainless steel foil was taken as an example to analyse the effects of target distance and time on the formation quality of array micro-pores. The feasibility of the process is verified and a new technology for micro plastic forming of metal foil is provided.

2 Experimental Device And Method

2.1 Experimental nozzle

The key part of producing cavitation of the cavitating water jet is the nozzle. The self-excited oscillating organ pipe nozzle is combined with the triangular nozzle in this paper, which largely enhances the shear effect and designs the mixed nozzle with stronger cavitation effect.

According to the theory of the converging nozzle, the diameter of the mixed throat is [16]

$$d = \left[\frac{Q}{0.658\sqrt{\overline{PM}}}\right]^{\frac{1}{2}} \times 1.05 - K$$

1

where Q is the inlet flow rate of the nozzle, P is the incident pressure, K is the correction factor of the nozzle, M is the outlet number of the nozzle.

The rated volume flow Q of the pump is 14 L/min, the rated pressure P is 20 MPa, the coefficient K is 0.6, the number of nozzle holes M is 1 and the diameter d of the mixed nozzle throat is 1.6 mm in this experiment.

Natural frequency of the nozzle cavity f depends on the inlet section ratio $(D_S/D)^2$ and the outlet section ratio $(D/d)^2$, where D_S is the diameter of the inlet cavity and D is the diameter of the resonant cavity:

$$f = KN\frac{a}{L}$$

2

where K_N, L and a are the modulus coefficient, the length of resonant cavity and the disturbance wave velocity of the resonant cavity, respectively.

The modulus coefficient K_N is

$$KN = F\{N, (\frac{Ds}{d})^2, (\frac{D}{d})^2\} = \begin{Bmatrix} \frac{2N-1}{4}[(\frac{Ds}{D})^2 >> 1, (\frac{D}{d})^2 >> 1] \\ \frac{N}{2}[(\frac{Ds}{D})^2 >> 1, (\frac{D}{d})^2 << 1] \end{Bmatrix}$$

3

where N is the oscillation modulus of the resonant cavity, N is 1, the inlet section ratio $(D_S/D)^2$ is 3.5-4.5, the outlet section ratio $(D/d)^2$ is 10-11.

When the natural frequency f of the mixing nozzle cavity is equal to the critical self-excited frequency f^*, the strongest resonance will occur. If the nozzle length is not limited, f^* is taken as a small critical Strouhal number.

$$f^* = S_d^* \cdot \frac{M_a}{d} \cdot a$$

4

where v is the exit velocity of the nozzle jet, a is the expansion angle, where M_a is the Mach number.

The most intense resonance occurs in the mixing nozzle with the strongest resonance, which should meet the following requirements:

$$\frac{L}{d} = \frac{K_N}{M_a S_d^*}$$

5

Figure 1 shows the structure of the mixing nozzle used in the experiment, and the expansion angle *a* of the common triangular nozzle is 40°.

2.2 Experimental device

The main composition of the experimental system is illustrated as shown in Fig. 2. TW-5570 ultra-high-pressure plunger pump is used as the high-pressure pump station. The acrylic resin water tank of 1,000 L contains purified tap water at 25±2℃ stored for at least 24 h.

The array experiment of micro-forming die is carried out on an annular array blind-hole with a diameter of Φ1.2 mm×3 mm and made by micro EDM. Its structure is illustrated as shown in Fig. 3 and the self-designed array micro-forming fixture structure used in the experiment is presented as shown in Fig. 4.

To ensure that the submerged cavitating water jet is not disturbed by the free surface, the distance between the vertical downward nozzle and the free surface of the water tank top is set to more than 300 cm. Referring to the previous experience of the cavitation water jet shot peening optimal target distance [17], the target distance is 100-140 mm, and the impact loading time is 1-5 min.

2.3 Experimental principle

The submerged cavitating water jet impinges on the target in three annular regions, the water jet impact zone within a certain range of the jet centre, the adjacent impact zone of cavitation collapse and the surrounding impact zone. When the incident pressure is 20 MPa, the action time is 5 min and the distribution of three annular regions of 2Al2 aluminum alloy with the change in target distance under the impact of cavitating water jet is roughly distributed as shown in Fig. 5.

Cavitation water jet is affected by nozzle shape, complex conditions, equipment and target distance in water. Strict boundaries are absent among the three impacting zones. Fig. 6 illustrates its working principle according to the theory of cavitation water jet. The high-speed jet from the nozzle is blocked by the surrounding liquid, the velocity of jet is decreasing and few vacuoles are found in the middle of the jet due to the small pressure change. The impact force of the annular belt in the water jet action zone is largely reduced. The external jet and dynamic jet shear strongly with the surrounding static water outside the centre. The pressure obviously changes and the number and development of cavitation are abundant. Therefore, the annular band is the strongest under the impact of cavitation collapse. Although a few vacuoles are outside the cavitation impact zone, it diffuses outwards with the jet flow, and its effect on the material is limited [18, 19].

3 Experimental Results And Analysis

3.1 Cavitation water jet array micro-forming

The plastic array micro-forming experiment was carried out on a 304 stainless steel foil with a thickness of 80 μm, length of 60 mm and width of 60 mm under the condition of a 120 mm target distance and 5

min action time.

The impact three-dimensional morphology cloud map randomly of Fig. 7(b) is selected in the hollow vacuoles collapse impact region in Fig. 7(a). The three-dimensional image of impact of Fig. 7(b) is randomly selected in the impact zone of vacuoles collapse in Fig. 7(a). Its cross-section shows the smooth profile, and the forming depth is uniform. No crack exists on the surface of the formed hole, and no wrinkle forms around the hole. Fig. 7(c) is a two-dimensional profile of all array micro-pores of a-f in the L_1 direction in Fig. 7(a). The forming depth of micro-pores a and i in the outer impact zone and micro-pores e and f in the water jet impingement zone is not ideal. The b-d and g-i micro-pores on the impact zone of vacuoles collapse have good shapes, and the uniformity of forming holes and the consistency of the maximum forming depth are good. Good shape and surface quality can be obtained by this method for the foil plastic array micro-forming.

3.2 Effect of impact time on the micro-array forming

The impact time is one of the important parameters for the metal foil plastic array micro-forming by cavitating water jet. Therefore, the control target distance is 120 mm, and the inlet pressure is 20 MPa. The average depth and depth variance of a 304 stainless steel for all holes in the cavitation collapse impact zone are obtained with the curve of changed impact action time.

With the increase in impact action time, the depth of micro-hole increases, and the variance decreases as shown in Fig. 8. When the impact time was 1 min, the depth of the micro-pore was only 68.5 μm. However, when the impact time reached 5 min, the depth of the array micro-pore was increased to 159 μm. This phenomenon is due to the increase in time. The cavitation collapse and impact at the same position accumulate continuously, with the variation rule of array micro-pore depth obviously increasing and a surfacing variance which decreases with time. When the impact time increased from 1 min to 2 min, the array micro-pore depth increased by 34.5 μm. However, considering that the vacuoles collapse impact will produce an impact strengthening effect on the surface of the sample, the depth of the array micro-pores only increased by 12 μm in the process from 4 min to 5 min, with an increased forming difficulty.

Table 1
Average forming depth and standard deviation variation with forming time at the stand-off distance of 120 mm

Depth (μm)/Variance (μm)			
Time *t* (min)	*r*=10.2 mm	Time *t* (min)	*r*=10.2 mm
1	67.3/15.5	1	67.3/15.5
2	105.3/13.2	2	105.3/13.2
3	127.3/10.8	3	127.3/10.8
4	147.3/8.6	4	147.3/8.6
5	158.5/7.4	5	158.5/7.4

Aiming at the impact time of the array of micro-holes at different positions in the cavitation water-jet cavitation collapse impact zone on the depth and variance of the micro-holes, the arrays of micro-holes b, c and d in Fig. 7(a) are selected as the research objects, and its radii are respectively *r*=10.2 mm, 13.6 mm and 17 mm. Its mean and variance are taken to obtain the variance of array micro-pore depth at different radii in the vacuoles collapse impact region, which varies with the impact time as shown in Table. 1.

It can also be seen that increasing the impact time is helpful for improving the uniformity of the forming depth of the foil array micro-pores, and the array micro-pores at r=13.6mm have the largest depth and more uniform forming depth. Mainly because this corresponds to the position of the shear layer cavitation vortex ring, the cavitation moves rapidly downstream and collapses here. Which is consistent with the results of the researches in literature [17] and literature [20].

3.3 Effect of the target distance on the array micro-forming

The target distance of impact is another important parameter for the plastic array micro-forming of metal foil with cavitating water jet. Therefore, with the control pressure of 20 MPa and the impact time of 5 min, the average depth value and depth variance of all holes formed in the 304 stainless steel foil in the cavitation collapse impact zone are obtained as shown in Fig. 9.

With the increase in target distance, the depth of array micro-pores first increases and then decreases as shown in Fig. 9. When the target distance is *S*=120 mm, the micro-pore depth is obviously better than other target distances, and the variance of micro-forming depth under different target distances is similar, but the variance is small when the target distance is 120 mm. The main reason is that when the target distance is 120 mm, a large number of cavities are in the stage of concentrated collapse. When the target distance is bigger than 120 mm, the cavitation will collapse before reaching the target surface. Thus, the depth of micro-hole of the array decreases rapidly, and the uniformity of array-forming holes is poor.

Aiming at the influence of array micro-pore target distance at different positions in the cavitation collapse impact zone of cavitating water jet on the depth and variance of micro-pore, the arrays of micro-pores on the radii of b, c and d in Fig. 7(a) are *r*=10.2 mm, 13.6 mm and 17 mm are similarly selected as the

research objects. Then, the mean and variance are taken. The variation values of the depth and variance of the array micro-pore with target distance at different radii in vacuoles collapse impact zone are obtained as shown in Table. 2.

Table 2
Average forming depth and standard deviation variation with the stand-off distances at 5 min

	Depth (μm)/variance (μm)		
Target distance S (mm)	r=10.2 mm	r=13.6 mm	r=17 mm
100	76/9.5	85.4/8.2	89.4/8.6
110	136.2/7.7	147.5/6.9	145.5/7.9
120	158.9/7.3	166.2/5.9	156.5/7
130	141.2/7.5	151.8/6.6	149.8/8.1
140	58.3/7.8	74.6/7.2	66.8/8.2

The trend in the change of the depth and its variance of the array micro-pore with the same target distance are known. However, when the target distance is 120 mm, the array micro-pore depth values on all radii are the largest, and the variance is the smallest. The value depth of the array micro-pore at *r*=13.6 mm is the largest, reaching 166.2 μm. Furthermore, the minimum variance is only 5.9 μm, which indicates that the quality of the array micro-pore is the best at this position.

3.4 Surface roughness analysis of array micro-holes

The most commonly used contour arithmetic square variance (*Ra*) is used to characterise the roughness of the bottom of array micro-pore of the 304 stainless steel. Its *Ra* is

$$R_a = \frac{1}{n}\sum_{i=1}^{n}\left|z_i\right|$$

6

The original surface of the 304 stainless steel material is a measured roughness of three positions as shown in Fig. 10. The length is 132 μm and the original surface roughness is 0.507 μm.

Based on the previous study in the vacuoles collapse impact zone, the pressure of 20 MPa, the target distance of 120 mm, the impact time of 5 min and the 304 stainless steel material micro-holes are chosen as the object. The micro-holes of different radii are randomly selected, and the surface morphology of the bottom surface is observed as shown in Fig. 11. Compared with the roughness of the original surface, morphology such as an orange peel appeared on the bottom surface of the array micro-pores at all positions, and the rolling trace basically disappeared and the surface became somewhat coarsened.

To further examine the roughness variation rule of the surface of array micro-pores, the roughness of the surfaces of all the bottom parts of micro-pores with different radii was measured, and the average value was taken to obtain the surface roughness variation curve as shown in Fig. 12.

The mean roughness values of micro-pores of different radii are close to one another, which are all above 1.3 μm. The maximum roughness of micro-pores of radius r=13.6 mm is 1.54 μm, and the minimum roughness of micro-pores in radius r=17mm is 1.36 μm. The roughness is proportional to the depth of micro-pores. The larger the plastic deformation of the composite material, the more consistent the grain movement is with the macroscopic roughness.

3.5 Analysis for the thinning rate of array micro-pores

The thickness distribution of the array micro-forming holes in the impact zone of the sample was studied. The thinning of the material would lead to the risk of cracking, which would seriously damage the properties of the material. The cavitation bursting impact zone with the pressure of 20 MPa and the impact time of 5 min at a target distance of 120 mm is taken. A micro-hole of the inner radius r=13.6 is arbitrarily select and embed in epoxy. A digital microscope polished by sandpaper is used to measure the cross-sectional thickness as shown in Fig. 13.

Definition of the thinning rate of foil T:

$$T\ (\%) = \frac{t_0 - t_i}{t_0} \times 100\% \quad (7)$$

where t_0 is the initial thickness of the sample, t_i is the thickness of the measuring point of the forming hole.

Fifteen points were selected for the measurement. Owing to the vacuoles collapse impact, the material flow was difficult under the rigid contact constraint of the round corners of the micro-die; thus, the minimum thickness is 70.4 μm at the rounded corners of the micro-die. The restriction on the part from the rounded corners of the micro-die to the centre of the cavity is lack under the action of inertia effect, it tends to increase and then decrease. Fig. 14 illustrates the thickness distribution of the micro-pore section.

Figure 15 shows the variation of thinning rate of array micro-pores in different radii of vacuoles collapse impact zone of the 304 stainless steel foil under pressure of 20 MPa, target distance of 120 mm and impact time of 5 min. The thinning rates of the array micro-formed parts in the impact zone of vacuoles collapse are between 2% and 13.5%, and the variation trend of the thinning rate between the micro-formed holes at different positions is the same. However, the overall thinning rate of array micro-pores with radius r=13.6 mm is larger, and the maximum value is 13.375% at the rounded corner of micro mould. The overall thinning rate of array micro-pores on radius r=10.2 mm is smaller, but its maximum value also appears at the corner of micro mould, which is 10.75%. In addition, the thinning rates of all the

array micro-pores are generally between 2–10% except at the fillet, which indicates that the thickness distribution of the samples impacted by cavitating water jet is good.

4 Conclusion

A new method for the micro-forming of metallic plastic array is researched in this paper, which is based on the proposed submerged cavitation water jet and cavitation collapse shock wave. The feasibility of the technology is verified and an ideal array of 304 stainless steel micro-holes are obtained. The plastic array micro-forming is also analysed. The array micro-forming holes with good quality can be prepared by this technology. Results are as follows:

(1) The impact zone of vacuoles collapse is verified as the best micro-forming region of array. The forming depth and uniformity of array micro-pores change regularly with the impact time and target distance. The forming effect is the best when the impact time of array micro-holes is 5 min and at the position of radius r=13.6 mm and the target distance is 120 mm. Its mean deformation depth was up to 166.4 μm, and the variance was only 5.9 μm.

(2) When the shock waves generated by cavitation collapse are applied to the surface of the foil, the roughness of the array micro-pores is increased, and the maximum roughness Ra=1.54 μm. The thickness reduction rates of array micro-forming parts are generally between 2% and 10%. The maximum thinning rate is located at the rounded corner of the micro-die only 13.5% with the thickness of the section distributed evenly.

Abbreviations

D(mm)	Diameter of the resonant cavity
D_S(mm)	Diameter of the inlet cavity
f	Natural frequency of the nozzle cavity
f^*	Critical self-excited frequency
K	Correction factor of the nozzle
K_N	Modulus coefficient
L(mm)	Length of resonant cavity
M	Outlet number of the nozzle
N	Oscillation modulus of the resonant cavity
P(MPa)	Incident pressure
Q(L/min)	Inlet flow rate of the nozzle
Ra(μm)	Surface roughness
S_d^*	Small critical strouhal number
T	Thinning rate of foil
t_i(mm)	Thickness of the measuring point of the forming hole
t_0(mm)	Initial thickness of the sample
v(m/s)	Exit velocity of the nozzle jet
a	Disturbance wave velocity of the resonant cavity

Declarations

Compliance with Ethical Standards:

Funding: This study was funded by the financial support of the Six Talent Peak Selection and Training Program of Jiangsu (XNYQC-002), Jiangsu University Senior Talent Start-up Funds (16JDG038), Equipment Pre-Research Field Fund Project (80923010201), the opening foundation of the State Key Laboratory of Space Medicine Fundamentals and Application, Chinese Astronaut Research and Training Center (SMFA20K07), and National Natural Science Foundation of China (52105259).

Conflicts of Interest: The authors declare that they have no conflict of interest. The manuscript is approved by all authors for publication.

a. Funding

This study was funded by the financial support of the Six Talent Peak Selection and Training Program of Jiangsu (XNYQC-002), Jiangsu University Senior Talent Start-up Funds (16JDG038), Equipment Pre-Research Field Fund Project (80923010201), the opening foundation of the State Key Laboratory of Space Medicine Fundamentals and Application, Chinese Astronaut Research and Training Center (SMFA20K07), and National Natural Science Foundation of China (52105259).

b. Conflicts of interest/Competing interests

The authors declare that they have no conflict of interest. The manuscript is approved by all authors for publication.

c. Availability of data and material

Not applicable

d. Code availability

Not applicable

e. Ethics approval

Not applicable

f. Consent to participate

The authors declare that they have no known competing financial interests or personal relationships that could have appeared to influence the work reported in this paper.

g. Consent for publication

Not applicable

h. Authors' contributions

Not applicable

References

1. Fu MW, Chan WL (2013) A Review on the state-of-the-art micro-forming technologies. Int J Adv Manuf Tech 67(9–12):2411–2437. http://doi.org/10.1007/s00170-012-4661-7
2. Presz W, Kulik T (2019) Ultrasonic vibrations as an impulse for glass transition in micro-forming of bulk metallic glass. Arch Civ Mech Eng 19(1):100–113. http://doi.org/10.1016/j.acme.2018.09.001
3. Raja CP, Ramesh T (2021) Influence of size effects and its key issues du-ring micro-forming and its associated processes-A review. Eng Sci Technol 24(2):556–570. http://doi.org/

10.1016/j.jestch.2020.08.007

4. Frank V, Hu ZY et al (2004) State of the art in micro-forming and investigations into micro-deep drawing. J Mater Process Tech 151(1–3):70–79. http://doi.org/10.1016/j.jmatprotec.2004.04.266
5. Engel U, Eckstein R (2002) Micro-forming from basic research to its realization. J Mater Process Tech 125–126. https://doi.org/10.1016/s0924-0136(02)00415-6
6. Justinger H, Gerhard H et al (2005) Analysis of cup geometry and temperature conditions in the miniaturized deep drawing process. Advanced Technology of Plasticity, : 459-460. https://doi.org/10.4028/www.scientific.net/kem.344.791
7. Cao B, Meng B et al (2019) Research and application of energy field assisted micro-forming technology. J Netshape Form Eng 11(3):14–28. http://www.cnki.net
8. Koo SJ, Kim HS (2020) The homogeneity of multi-textured micro-pat-tern arrays in a laser shock surface patterning process and its effect on the surface properties of aluminum alloy. Surf Coat Tech 382:125149. http://doi.org/10.1016/j.surfcoat.2019.125149
9. Soyama H (2020) Cavitation peening: a review. Metals-Basel 10(2):270. http://doi.org/10.3390/met10020270
10. Lee MH, Lee KS et al (2012) On the synthesis of an underwater ship hull cleaning robot system. Int J Precis Eng Man 13(11):1965–1973. http://doi.org/10.1007/s12541-012-0259-0
11. Tao YQ, Cai J et al (2018) Experimental study on degradation-n of organic wastewater based on high pressure cavitating jet impingement. J. Eng. Thermophys. 39(12): 2738-2744. http://doi.org/0253-231X(2018)12-2738-07
12. Wang RH, Wan CH et al (2019) Mechanism of heavy oil viscosity reduction by cavitation jet. J China Univ Petroleum 43(5):101–108. http://doi.org/10.3969/j.issn.1673-5005.2019.05.011
13. Tsuda H, Ju DY et al (2005) Residual stress in a quenched gear shaft treated by water cavitation peening. Mater. Sci. Forum. 490-491: 364-369. http://doi.org/10.4028/www.scientific.net/MSF.490-491.364
14. Soyama H, Saito K (2003) Peen forming of duralumin plate by using a cavitating jet in air. Proceedings of the 7th Pacific Rim International Conference on Water Jetting Technology. : 429-436. http://doi.org/ 10.1299/jsmetohoku.2004.40.201
15. Chen TN, Guo ZN et al (2017) Experimental research and numerical simulation of the punch forming of aluminum foil based on a laser induced cavitation bubble. Int J Adv Manuf Tech 93(1):1–10. http://doi.org/ 10.1007/s00170-017-0741-z
16. Li GS, Shen ZH (2008) Theory and application of free-vibration cavitation jet. China University of Petroleum Press
17. Li FZ, Tan ZR et al (2019) Study on dynamic evolution o-f cavitation clouds and optimization of standoff distance in water cavitation peening. Chin J Mech Eng-En 55(9):120–128. http://doi.org/10.3901/JME.2019.09.120

18. Nayebzadeh A, Wang YY et al (2017) Cavitation behind a circular micro pillar. Int J Multiphas Flow 9(8):67–78. http://doi.org/10.1016/j.ijmultiphaseflow.2017.08.012
19. Peng GY, Oguma Y et al (2016) Numerical analysis of cavitation cloud shedding in a submerged water jet. J Hydrodyn 28(6):986–993. http://doi.org/10.1016/S1001-6058(16)60700-X
20. Wu Q, Wei W et al Dynamic characteristics of the cavitation clouds of submerged Helmholtz self-sustained oscillation jets from high-speed photography [J].J Mech Sci Technol. http://doi.org/10.1007/s12206-019-0117-4

Figures

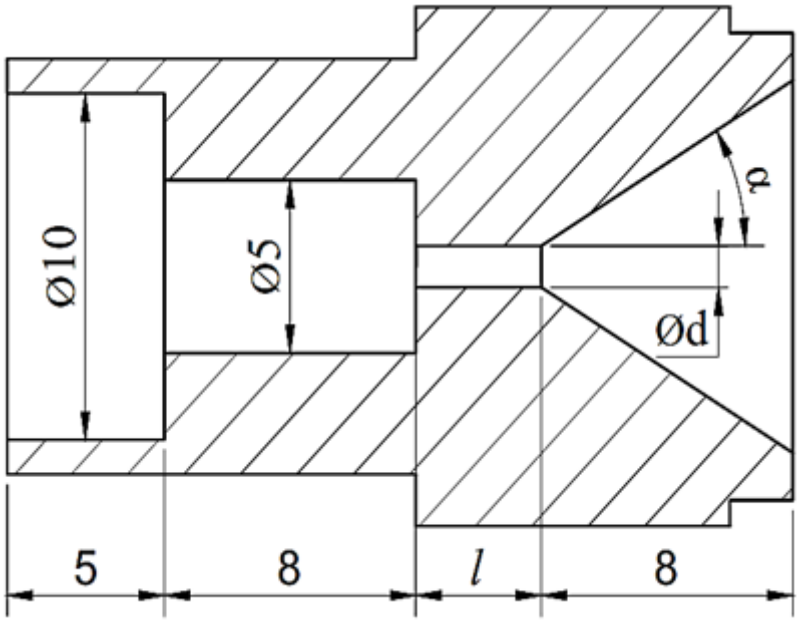

Figure 1

Structure of the mixing nozzle

Figure 2

Water-jet cavitation experimental system

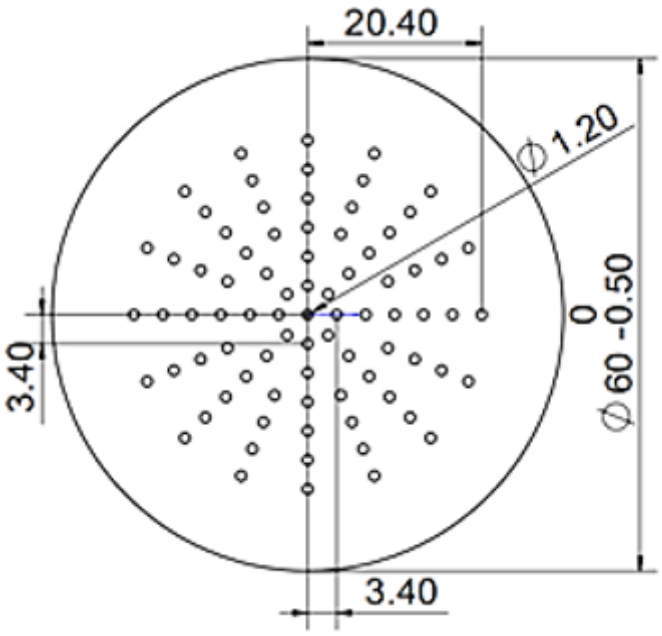

Figure 3

Shape and dimensions of the micro-mould

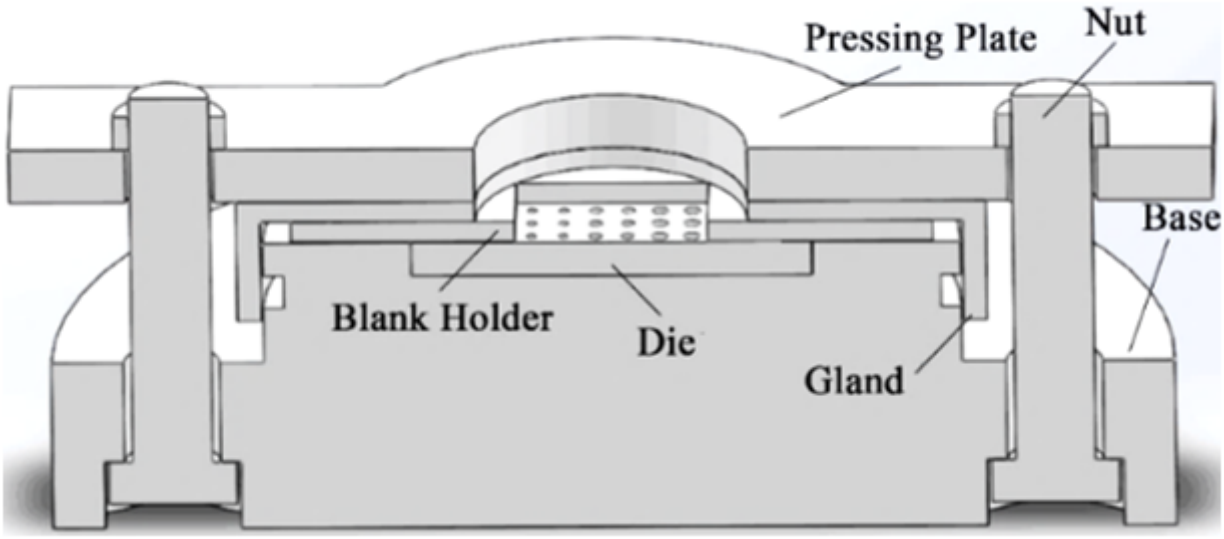

Figure 4

array micro-forming fixture

Figure 5

Distribution of the impinging area of submerged cavitating water jet with the change in target distance

Figure 6

Schematic diagram of foil array micro-forming impacted by submerged cavitating water jet

Figure 7

Plastic array micro-forming of the 304 stainless steel foil (a) Macroscopic morphology of the sample; (b) Three-dimensional topography of hole; (c) Micro-pore contour map in L_1

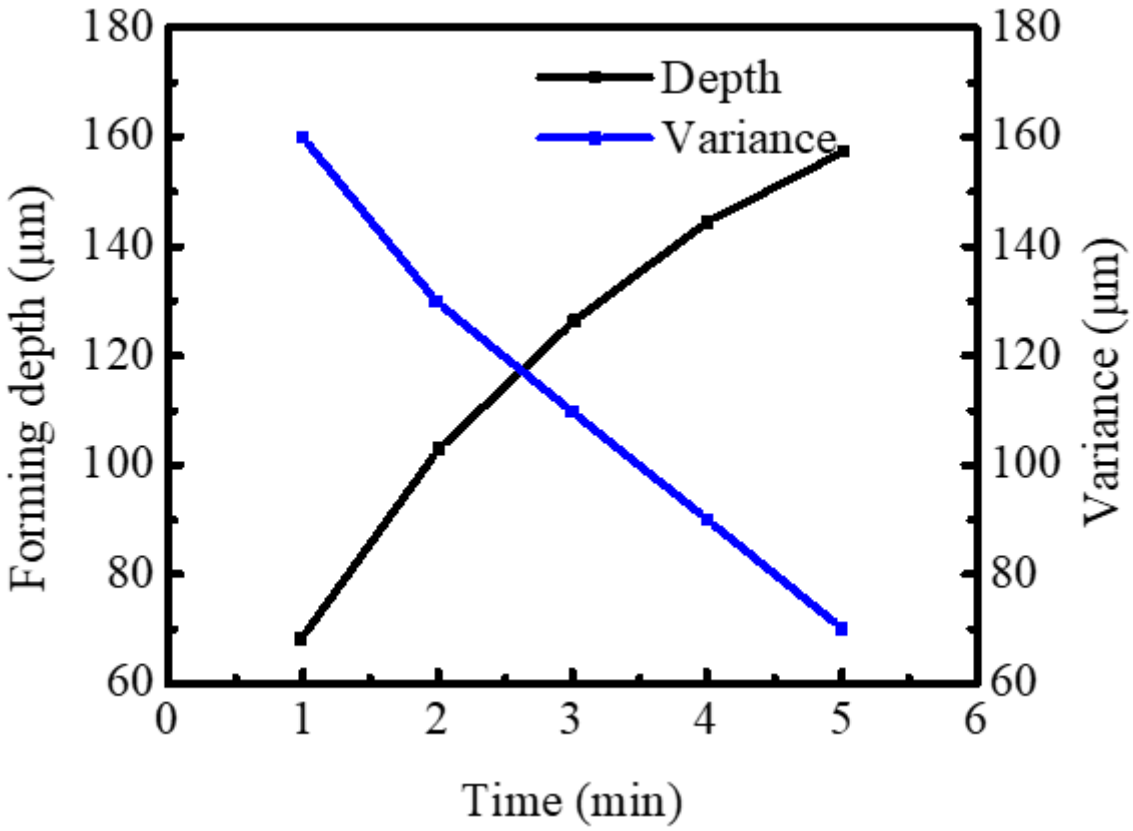

Figure 8

Influence of cavitation water-jet impact time on forming depth and variance

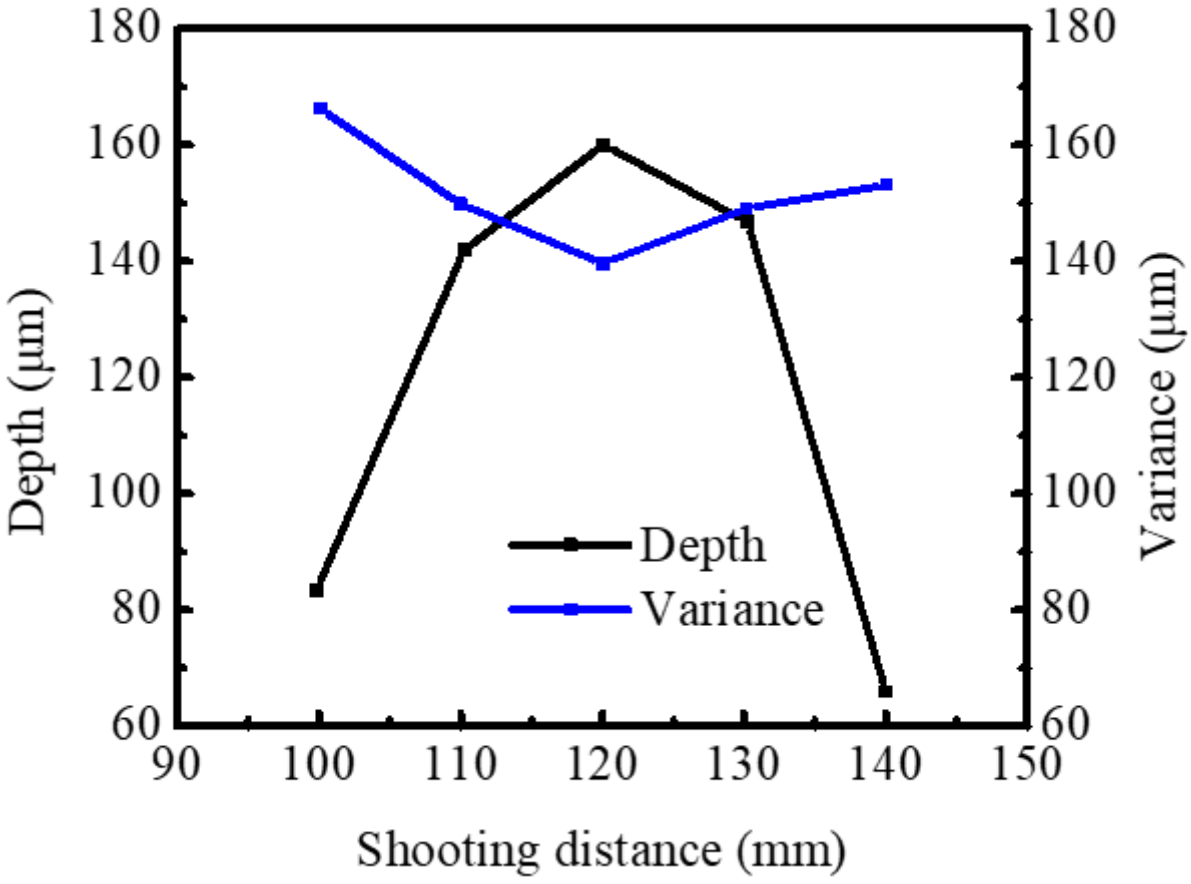

Figure 9

Influence of the standard distance on the forming depth and variance

Figure 10

(a) Measurement of surface roughness; (b) Roughness data sheet; (c) Line 1 roughness curve

Figure 11

Macro morphology of the bottom of micro-pore under different time conditions

Figure 12

Roughness of the bottom area of the bulging parts with different times

Figure 13

Schematic of the measurement locations of thickness distribution

Figure 14

Cross-section thickness distribution of the formed

Figure 15

Cross-section thickness distribution of the formed